



The Effect of Tip Clearance Kaplan Ducted Propeller in Offshore Supply Vessel (OSV) on Hydrodynamics

Arif Winarno^{1*)}, Gedhe Angkoso Nur Sofa Sakti¹⁾, Erik Sugianto¹⁾

¹⁾Department of Marine Engineering, Universitas Hang Tuah, Surabaya 60111, Indonesia

^{*)}Corresponding Author: arif.winarno@hangtuah.ac.id

Article Info	Abstract
<p>Keywords: Ducted Propeller; Tip Clearance; Thrust; Torque; CFD;</p> <p>Article history: Received: 27/06/2024 Last revised: 08/09/2024 Accepted: 12/09/2024 Available online: 31/10/2024 Published: 31/10/2024</p> <p>DOI: https://doi.org/10.14710/kapal.v21i3.64772</p>	<p>A ducted propeller is a modification of a propeller by adding a duct or nozzle. The purpose of using a ducted propeller is to increase thrust, increase propeller efficiency, and encourage better ship movement. This is suitable for Offshore Supply Vessel (OSV) vessels operating on offshore platforms to support oil drilling activities. In designing a kort nozzle, one of the most important components is the tip clearance, the distance between the edge of the propeller and the inner nozzle. The diameter of the kort nozzle can affect the thrust efficiency of the propeller. Due to the blade momentum theory for ducted propellers, the volume of water passing through the propeller should be as large as possible, with the smallest possible flow velocity. In this study, numerical simulations using the Computational Fluid Dynamics (CFD) method were carried out to determine the effect of tip clearance on thrust and torque on a ducted propeller with a MARIN foil 19A nozzle type and tip clearance of 10 mm, 20 mm, and 30 mm. From all models, the highest thrust and torque values were obtained from the nozzle 19A tip clearance 10 mm model with thrust 367,413 kN and torque 315,338 kNm. The relationship between tip clearance and thrust is inversely proportional; the greater the tip clearance, the smaller the value of thrust, and the same is true with torque.</p> <p>Copyright © 2024 KAPAL: Jurnal Ilmu Pengetahuan dan Teknologi Kelautan. This is an open access article under the CC BY-SA license (https://creativecommons.org/licenses/by-sa/4.0/).</p>

1. Introduction

There are several factors to consider when designing a ship for optimal efficiency, with the propulsion system being one of the key elements. Central to this planning is the design of the propeller, as an effective design allows for more efficient power transfer from the main engine [1]. A well-designed hull provides numerous advantages, including improved hydrodynamic performance. An efficient hull design should also minimize drag, which is essential for achieving optimal speed [2]. As the ship's speed increases, the Reynolds number also rises. [3] Initially, the water flow around the hull remains laminar, but as the ship accelerates, turbulence begins to form [4].

One method to enhance propulsion efficiency is the use of a Kort nozzle propeller, or ducted propeller, which has demonstrated an increase in the thrust force generated by the propeller [5]. Thrust, produced by the lift at the propeller's rear, moves in the same direction as the ship. To achieve optimal thrust, factors such as the number of blades, the pitch, and the blade profile must be considered [6]. Additionally, the positioning of the propeller shaft is crucial for channeling water flow from the bow to the stern, thus improving propeller efficiency [7].

The Kort nozzle, a foil-like plate designed to protect the propeller, helps to increase and direct water flow towards the propeller, enhancing the volume of water drawn in [8]. According to Oosterveld [9], there are two main types of duct cross-section profiles: accelerating ducts and decelerating ducts. Accelerating ducts aim to increase the flow velocity towards the propeller, while decelerating ducts aim to decrease it. The forces acting on the nozzle, influenced by its shape and operating conditions, can result in either positive or negative axial forces, contributing to or detracting from the total thrust of the system [10].

The inclusion of a duct around the propeller serves to increase thrust and direct water flow, enhancing the volume of water passing through the propeller. This design also helps to reduce cavitation at the blade tips due to the duct's presence [11]. For increased efficiency, the propeller and inner nozzle should be larger, and the gap between the propeller edge and the inner nozzle port should not exceed 0.75 of the propeller radius [12].

There are many different propeller types that can be used to customize the propeller design for different types of vessels. One of the best propeller types for large-powered vessels with low sailing speeds is the Kaplan series [13]. In terms of kort nozzle design, the tip clearance of a ducted propeller affects its efficiency and thrust; the larger the tip clearance, the less thrust and torque [14].

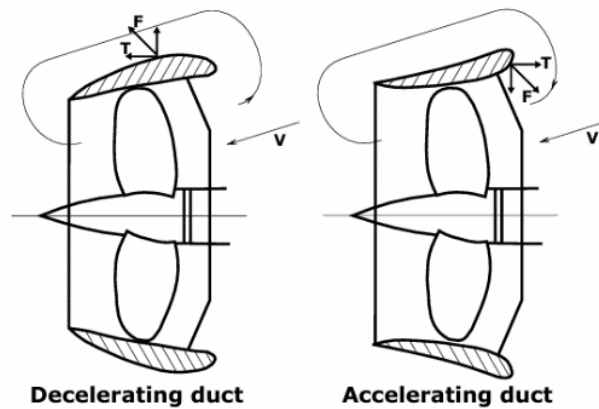


Figure 1. Sketch of an accelerating and a decelerating ducted propeller

Research conducted by Hermawan [15] and Ahmidila [16] reveals that the operational condition of the OSV 80 ship in the field has led to decreased performance due to frequent propeller losses, resulting in reduced ship speed. Additionally, OSV vessels require significant ship motion and thrust to effectively support offshore oil drilling activities. Implementing a Kort nozzle could potentially improve propeller thrust [17].

Upon identifying these issues, it is crucial to implement a solution to enhance the OSV 80 ship's performance. This study aims to determine the effect of the tip clearance of the Kort nozzle on the power and speed of the Kaplan propeller used on the OSV vessel. Three models of the MARIN foil nozzle 19A, with tip clearance values of 10 mm, 20 mm, and 30 mm (Similarly, Yongle et al (2015) conducted a numerical study of the effect of tip clearance on ducted propeller performance using tip clearance variations of 0.42%, 0.84%, and 1.25% of the propeller diameter [14]), were tested with the Ka-40 propeller on the OSV 80. This particular foil nozzle is advantageous due to its ease of production and fabrication [18].

2. Methods

The following are some of the steps that will be carried out in this research:

2.1. Literature Study

The goal of this step is to compile a summary of the existing theoretical foundation, supplemented with additional references and data for validation.

2.1.1. Force Drag and Force Lift

According to Popov [19], drag and lift forces arise when stress is multiplied by the stress area. However, these forces must be balanced or equal on the hypothetical object. The magnitude of the resulting force consists of shear stress, denoted by the symbol " τ " (tau), which acts parallel to the base plane area. This can be calculated using eq. (1).

$$\tau = \lim_{A \rightarrow 0} \frac{\Delta V}{\Delta A} \quad (1)$$

Thus, the mathematical formula for the drag force from eq. (1) can be expressed by eq. (2):

$$F_{drag} = \tau \times A \quad (2)$$

However, eq. (2) can be used to derive a mathematical formula with eq. (3) for the lift force:

$$F_{lift} = P \times A \quad (3)$$

Here, F_{drag} represents the drag force, F_{lift} represents the lift force, τ denotes wall shear, P stands for pressure, and A represents the area.

2.1.2. Thrust and Torque

Blade Element Momentum Theory (BEMT) is a methodology that integrates blade element theory and momentum theory to determine the forces acting on a propeller or turbine. The combination of these two theories provides a solution to the issues that arise when calculating rotor speed, as illustrated in Figure 2. Blade element theory, which originated from the initial development of finite wing theory, has traditionally been analyzed using a lifting line approach. This method considers the blade element as a two-dimensional foil, where the forces are analogous to those observed in a uniform two-dimensional flow with the same velocity and direction as those occurring locally on the blade element [20].

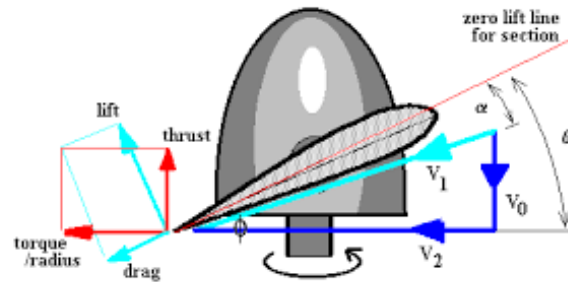


Figure 2. Force acting on the blade (Source: Syamsudin et al, 2018)

The propeller generates thrust force, which provides the necessary momentum for the ship's movement. By utilizing the blade element theory of momentum, which combines blade element theory with momentum theory, we can determine the force acting on the propeller using eq. (4) and (5), where T represents thrust and θ represents pitch.

$$F_z = F_L \cos \theta - F_D \sin \theta \quad (4)$$

$$F_x = F_L \sin \theta + F_D \cos \theta \quad (5)$$

The thrust equation of the blade momentum element theory is eq. (6):

$$T = F_{Lift} \cos \theta - F_{Drag} \sin \theta \quad (6)$$

Torque refers to the capacity of an object, such as a propeller, to rotate in a way that it turns on its axis. To calculate torque, you need to multiply the force (F) by the moment arm, which is expressed in eq. (7), where torque (τ) is given by the product of force (F) and moment arm (r).

$$\tau = F \times r \quad (7)$$

Using blade element theory, the momentum equation can be derived when torque acts on the blade, as outlined in eq. (8), where Q stands for torque and θ represents pitch.

$$Q = (F_{Lift} \cos \theta + F_{Drag} \sin \theta) \times r \quad (8)$$

To determine thrust and torque, the pitch angle must be calculated using the P/D ratio from eq. (9). The pitch angle derived from this value is used in further calculations.

$$\theta = \tan^{-1} \frac{P/D}{0,7\pi} \quad (9)$$

2.2. Collecting Data, Modelling, and Computational Fluid Dynamics

This research draws on data from previous studies, focusing on an Offshore Supply Vessel (OSV) equipped with a Kaplan Ka-40 propeller. Additionally, a MARIN nozzle foil is used to align the Kort nozzle, based on the reference "Marine Propellers and Propulsion" by John Carlton [18], nozzle coordinate data can be obtained from this reference. The percentage of the duct length (L or L_d value) is presented in the ordinate data, as shown in Table 1. Data was gathered from various sources, including online databases and prior research, to examine the impact of a Kort nozzle on a Kaplan-type propeller on an Offshore Supply Vessel (OSV).

Data for the Offshore Supply Vessel 80 (OSV) is sourced from earlier studies. The vessel has an overall length (LOA) of 40 meters, a waterline length (LWL) of 38 meters, a length between perpendiculars (LBP) of 36.8 meters, a beam (B) of 11.4 meters, a height (H), a draft (T) of 4 meters, and a service speed (V_s) of 13 knots.

Based on the collected data, the chosen option is to install a Ka-40 propeller with a 5° rake angle. The dimensional characteristics of this propeller align with the optimal findings from previous studies. Consequently, the propeller will be designed with a nozzle.

At first, a Ka-40 propeller model was created with the predefined parameters, and then a nozzle was added. The process began by detailing all elements, including the extended blade, pitch diagram, project development and outline, and side view and dimensions of the Kaplan propeller. With a propeller diameter of 2.4 meters, a propeller efficiency of 0.56, a propeller rotation speed of 300 rpm, and a propeller pitch of 0.65.

The propeller dimensions provided here reflect the best specifications based on prior research. The process involves modeling the Ka-40 propeller according to specified parameters, followed by modeling the same propeller with the addition of a nozzle.

The L_d value needed to determine the nozzle coordinates during the nozzle geometry manufacturing process is derived from the L_d/D ratio. The duct diameter (D) is calculated by adding the propeller diameter to the tip clearance corresponding to the chosen variation. Multiplying the L_d/D ratio by the duct diameter (D) gives the L_d value used for creating nozzle coordinates. For the 19A Kort nozzle model, the L_d value is 0.5.

The next step is to create a model after obtaining the necessary data. The 2D model was created with AutoCAD, and the 3D model was created with Rhinoceros. After that, simulations were performed using Ansys Fluent with meshing. Geometry, mesh, setup, solution, and result are the components of the project scheme, A pressure-based steady Reynolds stress solver is used for viscous models, suitable for rotating systems [24].

Table 1. Kort Nozzle Data
Duct Profile No. 19A

	LE																	TE	
x/L	0	1,25	2,5	5	7,5	10	15	20	25	30	40	50	60	70	80	90	95	100	
y_i/L	18,25	14,66	12,8	10,87	8	6,34	3,87	2,17	1,1	0,48	0	0	0	0,29	0,82	1,45	1,86	2,36	
y_u/L	0	20,72	21,07	20,8	Straight line													6,36	6,36

3. Results and Discussion

3.1. Modelling, Meshing, Setup, and Solution

The hull and propeller geometry of the Kaplan model were created using AutoCAD software based on data from previous studies [15] [21]. This is shown in Figure 3. Prior to initiating the simulation with Computational Fluid Dynamics (CFD) software, the first step is to create the OSV ship model. This is done using AutoCAD software to create a 2-dimensional design and Rhinoceros software to create a 3D model.

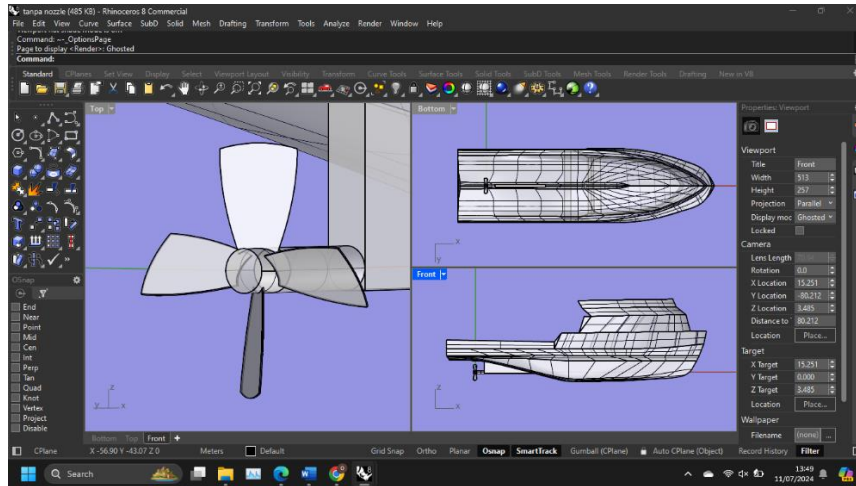


Figure 3. 3D geometry of OSV and propeller

Model geometries of the 19A kort nozzle with tip clearances of 10 mm, 20 mm, and 30 mm have been coupled with Kaplan propellers using Rhinoceros software. The following is a depiction of the 19A model geometry with a tip clearance of 10 mm that has been formed into a solid form using Rhinoceros software. In making the 3D model, the Ka-40 type propeller has been combined with each nozzle. The 19A 10 mm model has a nozzle length of 1200 mm and a tip clearance of 10 mm, as shown in Figure 4. On the left side of the image, the 3D geometry of the 19A 10 mm model is shown.

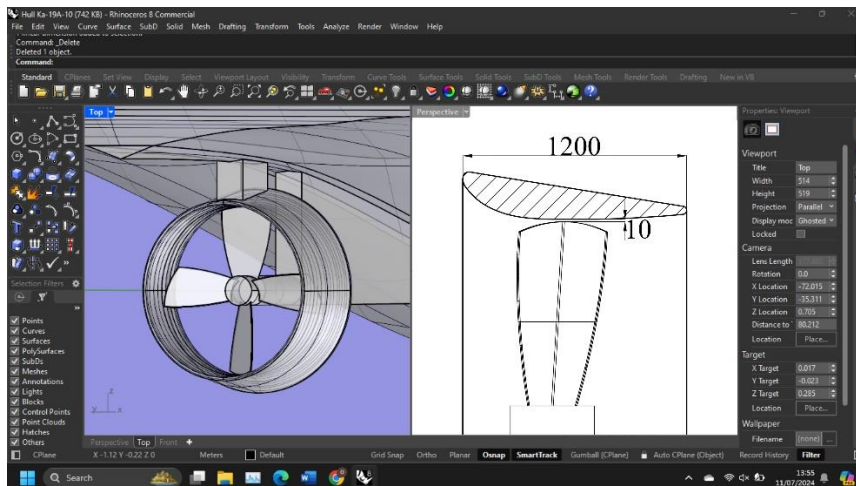


Figure 4. Geometry of kort nozzle model 19A 10 mm

The geometry of the 19A model with a tip clearance of 20 mm has been converted into a solid form using Rhinoceros software. The 19A 20 mm model has a nozzle length of 1200 mm and a tip clearance of 20 mm, as shown in Figure 5.

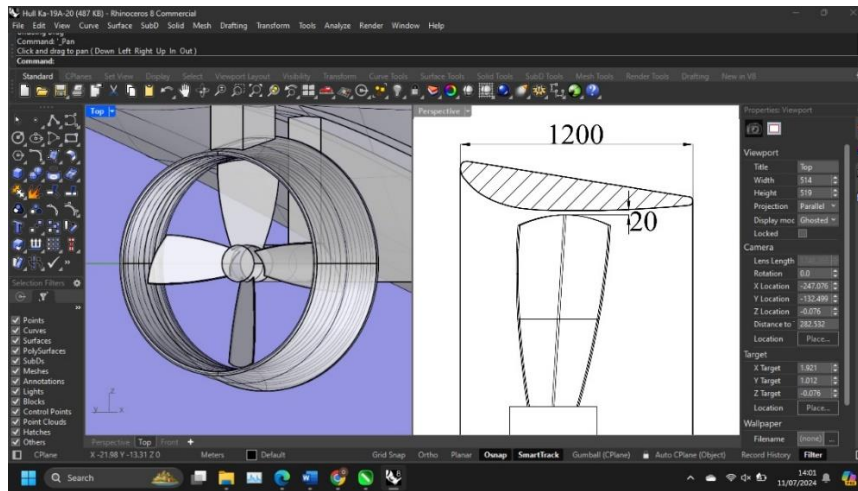


Figure 5. Geometry of kort nozzle model 19A 20 mm

The geometry of model 19A with a tip clearance of 30 mm has been converted into a solid form using Rhinoceros software. This 19A 30 mm model has a nozzle length of 1200 mm and a tip clearance of 20 mm, as shown in Figure 6.

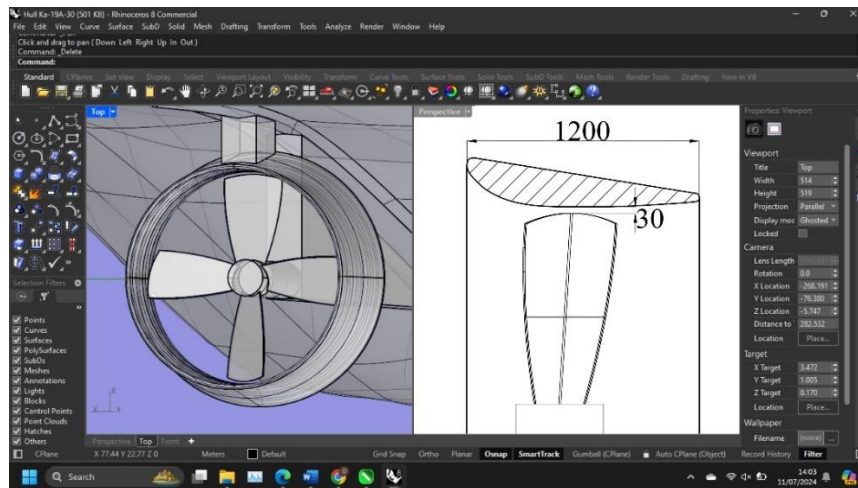


Figure 6. Geometry of kort nozzle model 19A 30 mm

The first step in the geometry phase involves importing the model from Rhinoceros software into SpaceClaim within Ansys. After ensuring all models have the necessary surfaces, the next step is to create the experimental domain. This study divides the experimental domain into two sections: a fluid domain and a rotating domain. The fluid domain, which resembles a pool, serves as the testing area to observe fluid phenomena around the hull. Refer to Figure 7 for more details about this region [21].

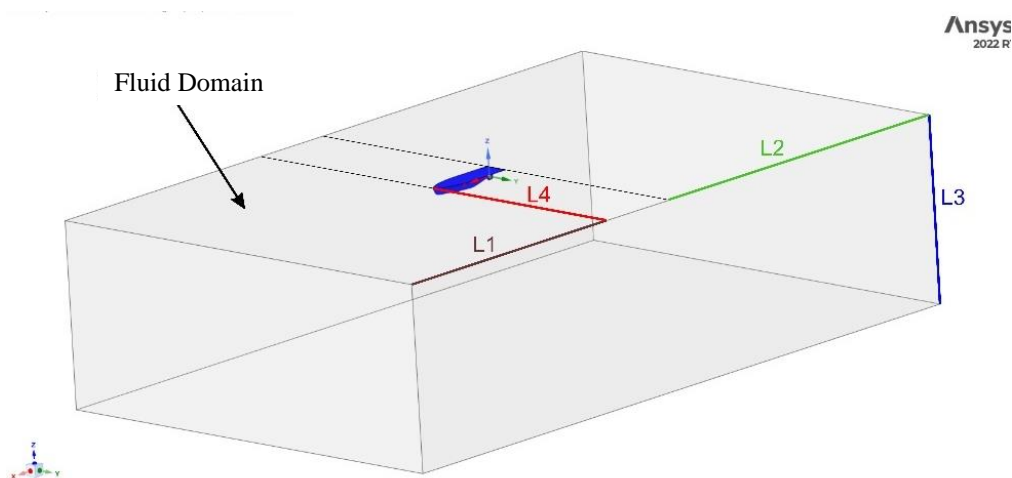


Figure 7. Fluid Domain

The dimensions of the fluid domain are as follows [27]: the length from the bow to the leading edge of the Lpp x 4 domain is 120 m (L1), the length from the stern to the trailing edge of the Lpp x 3 domain is 160 m (L2), and the length from

the stern to the bottom of the $L_{pp} \times 2.5$ domain is 80 m (L3). Additionally, the length from the stern to both the left and right sides of the $L_{pp} \times 2$ domain is 100 m (L4).

Regarding the rotating domain, this area will be defined around the propeller in its rotating state. For details on the dimensions of the rotating domain, please refer to Figure 8 [22].

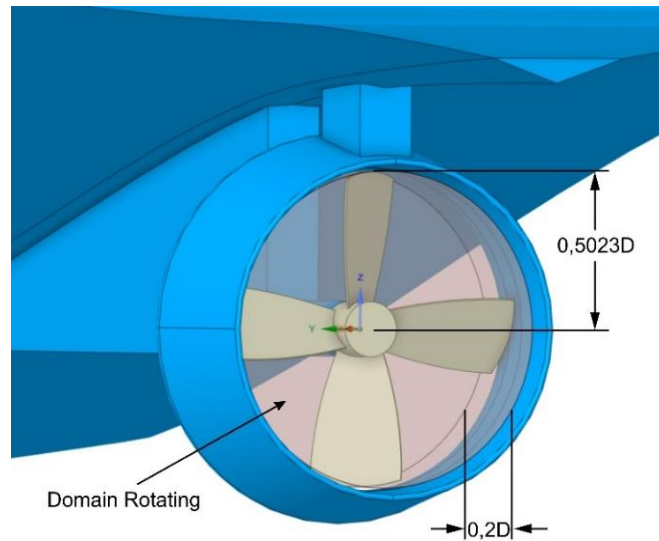
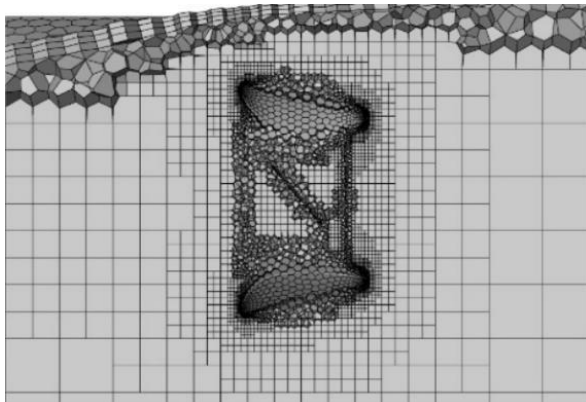


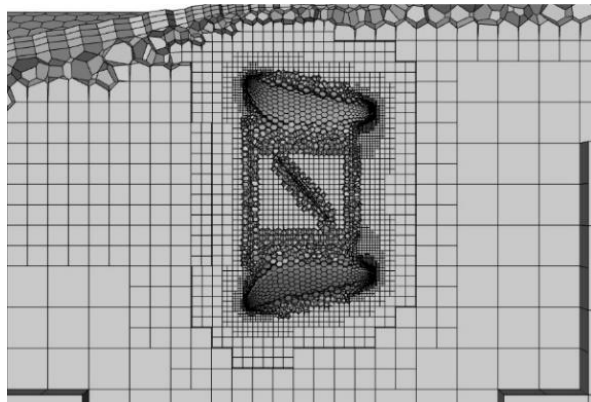
Figure 8. Rotating Domain

This stage is the most important in grid independence because it determines the right mesh variation by changing the face size and number of cells without affecting the simulation results. The mesh size and number of elements used will affect the time required. The smaller the mesh size and the greater the number of elements, the longer the network process will take. Using the optimal mesh size and number of elements will result in a very small and dense network, which allows for optimal results and increased accuracy when running simulations.

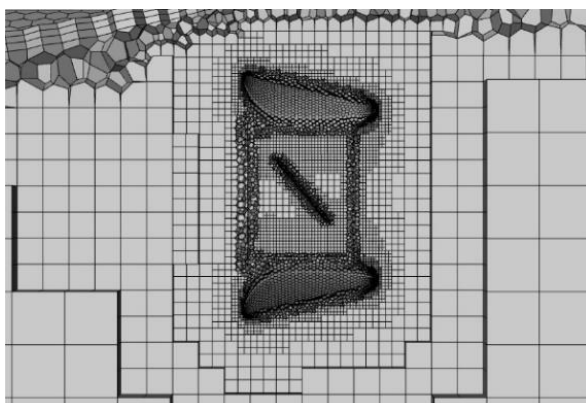
The mesh variation with a propeller and duct face size of 0.08 m produces 1,632,125 cells, as shown in Figure 9 (a). The mesh variation with a propeller face and duct size of 0.06 m produces 1,737,614 cells, as shown in Figure 9 (b). Mesh variation with a propeller face and duct size of 0.0365 m produces 1,898,489 cells, as shown in Figure 9 (c). Mesh variation with a propeller in Figure 9 (d) with a with a face and duct size of 0.035 m produces 1,953,235 cells. Mesh variation with a propeller face and duct size of 0.0345 m produces 1,991,073 cells, as shown in Figure 9 (e).



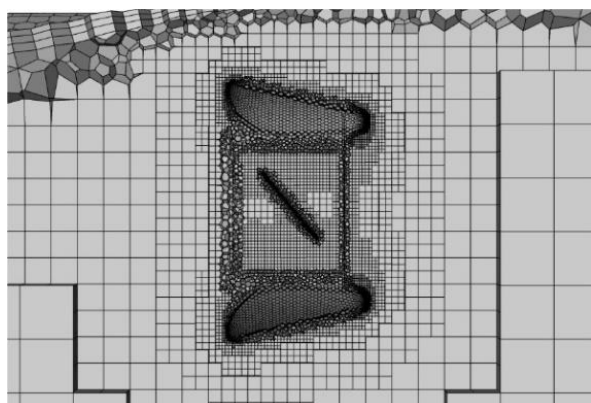
(a). Facesize 0,0800 m



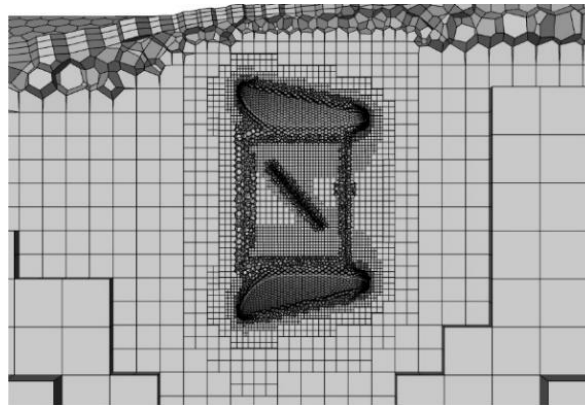
(b). Facesize 0,0600 m



(c). Facesize 0,0365 m



(d). Facesize 0,0350 m



(e). Facesize 0,0345 m

Figure 9. Propeller & duct facesize variation for grid independence

The results of meshing and setting are then collected in the form of thrust, as shown in Table 2.

Table 2. Thrust results from mesh variation

Face size (m)	cells	Thrust (N)
0,0800	1.632.125	369.878,97
0,0600	1.737.614	367.257,69
0,0365	1.898.489	367.005,07
0,0350	1.953.235	364.292,67
0,0345	1.991.073	365.248,44

The data in Table 2 can be presented in the form of thrust versus number of cells graph shown in Figure 10. It can be seen that at the number of cells from 1,632,125 to 1,991,073, thrust decreases and tends to stabilize with the addition of the number of cells up to 1,991,073. It can be concluded that using a mesh with a cell count of 1,991,073 or more will produce relatively the same resistance. The choice of mesh to be used is a face size of 0.035 m because the total thrust value does not exceed 5% of the largest thrust, which is in the mesh variation with a face size of 0.0345 m. The minimum mesh size is 50 mm, and the maximum is 1000 mm. The "improve surface mesh" process was used to correct mesh skewness to 0.6. The fluid and rotating domains are designated as fluid regions. Poly-hexcore meshing was used for volume meshing to minimize the number of cells formed [23].

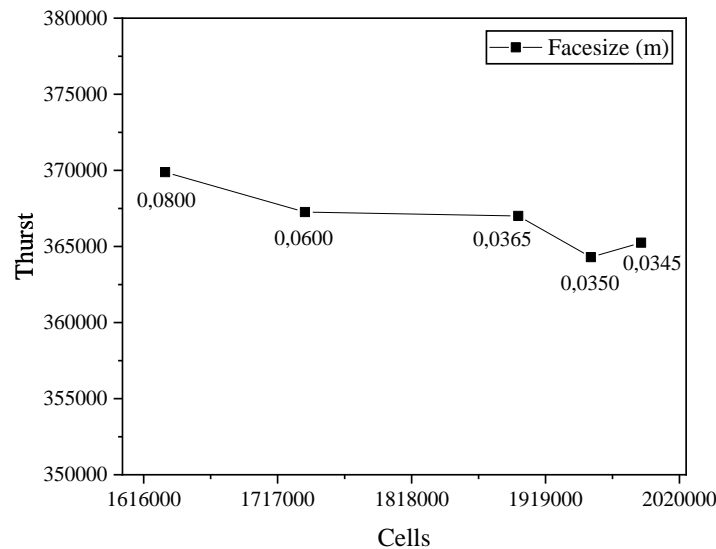
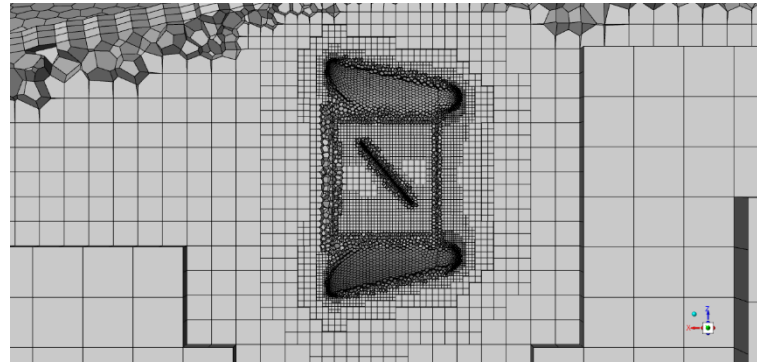
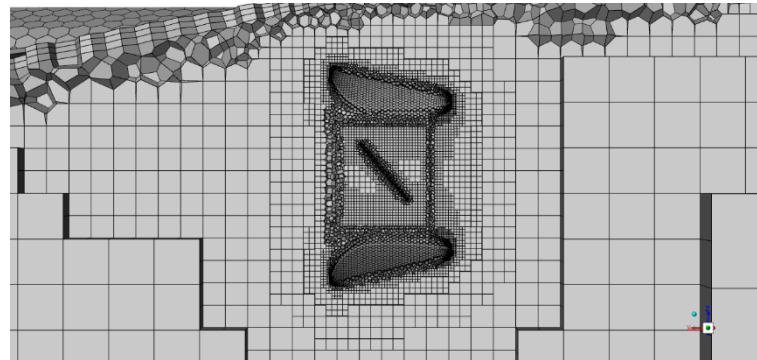


Figure 10. grid independence, thrust vs cells graph

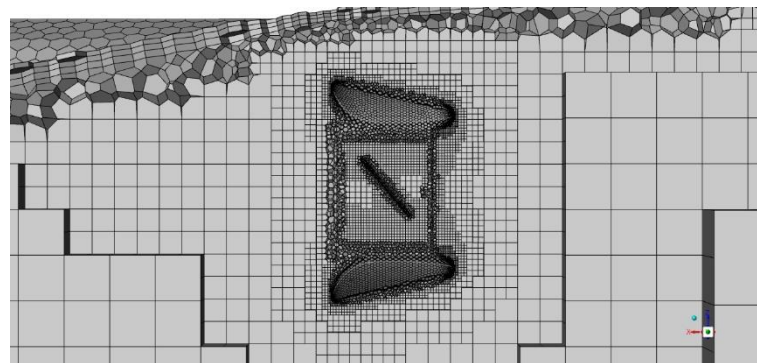
The meshing difference between each model (10 mm, 20 mm, 30 mm) is shown in Figure 11.



(a)



(b)

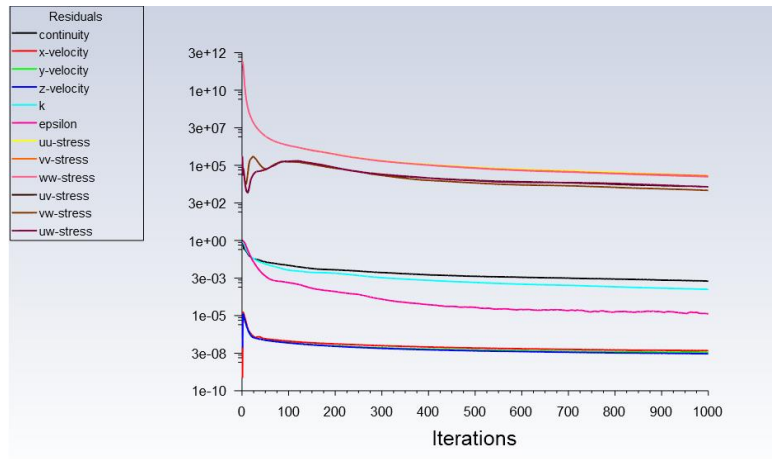


(c)

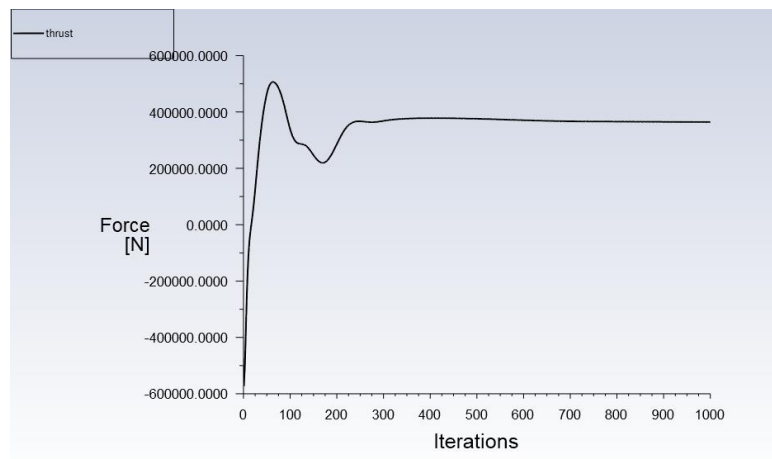
Figure 11. Meshing (a) 10 mm (b) 20 mm (c) 30 mm

The next step involves configuring the simulation parameters. During this phase, the parameters are adjusted for various conditions, including inlet, wall, outlet, ship, duct, and propeller boundaries, in line with the model specifications to be tested. The inlet condition specifies the incoming fluid flow, while the outlet condition represents the outgoing fluid flow. The wall boundary condition marks the pool's bottom and sides, whereas the ship boundary refers to the hull surface that can affect fluid flow in the simulation. A pressure-based steady Reynolds stress solver is used for viscous models, suitable for rotating systems [24]. In the cell zone condition, the rotating domain is defined as water (with a rotational velocity of 300 rev per minutes) and the fluid domain. The inlet velocity is set to 6.7 m/s, and the propeller is defined as a rotational moving wall for boundary conditions.

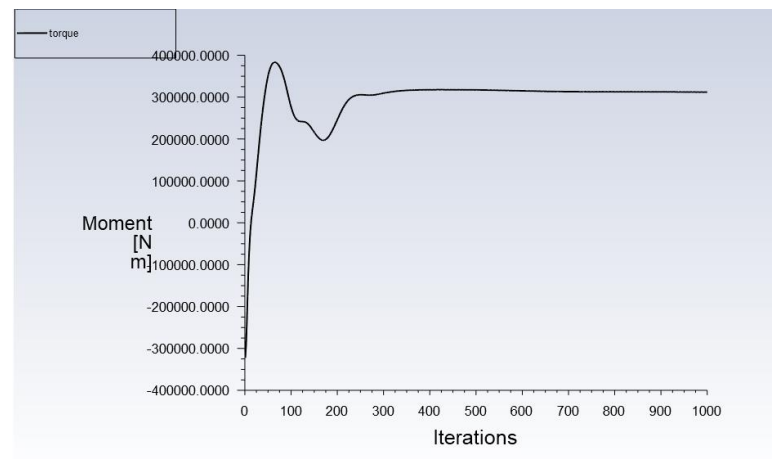
Once the setup is complete, the solution process is initiated. Figure 12 (a) shows the residuals graph of the numerical simulation, indicating how each residual component decreases with the number of iterations. Residuals measure the error in the numerical solution, decreasing as the process iterates until the solution converges or reaches a steady state. Residual values approaching very small numbers (close to $1e-10$) suggest that the solution is sufficiently convergent and stable. Some components, such as k and ϵ , may need further iteration or numerical parameter adjustments to achieve better convergence. Overall, this graph demonstrates that the simulation model has achieved convergence for most parameters after approximately 1000 iterations, this is the same as shown in Figure 12 (b) and Figure 12 (c), though some components may still require further refinement for complete stabilization. The results of this solution process are shown in Figure 12 (b), which depicts a graph with iterations on the x-axis and thrust in Newtons (N) on the y-axis, and Figure 12 (c), which shows torque (Nm).



(a)



(b)

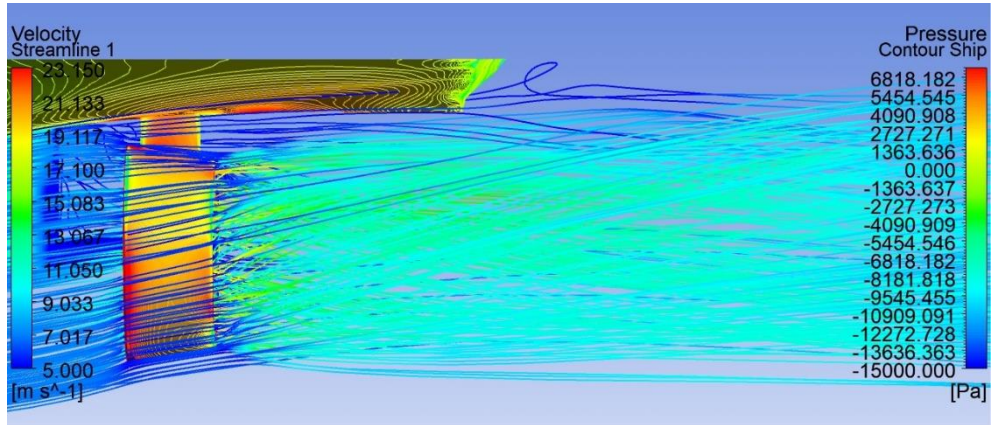


(c)

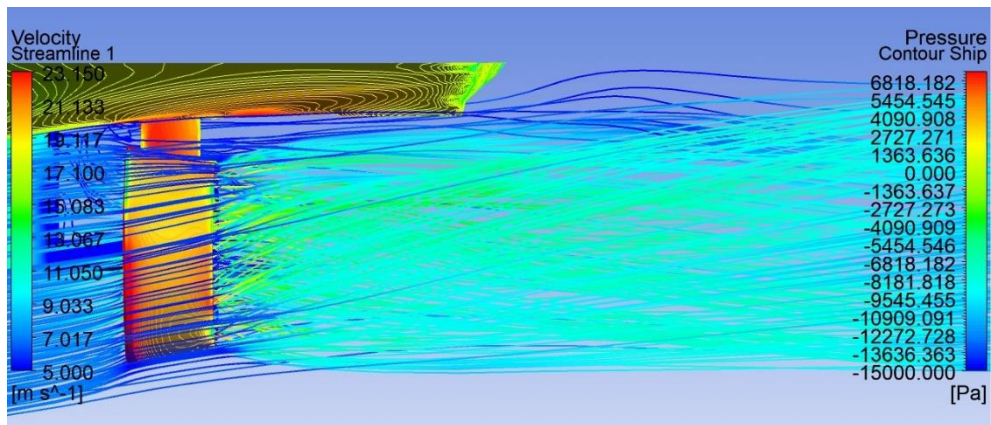
Figure 12. Results of solution (a) residuals (b) thrust (c) torque nozzle 19A tip clearance 20 mm

3.2. Result and Data Processing

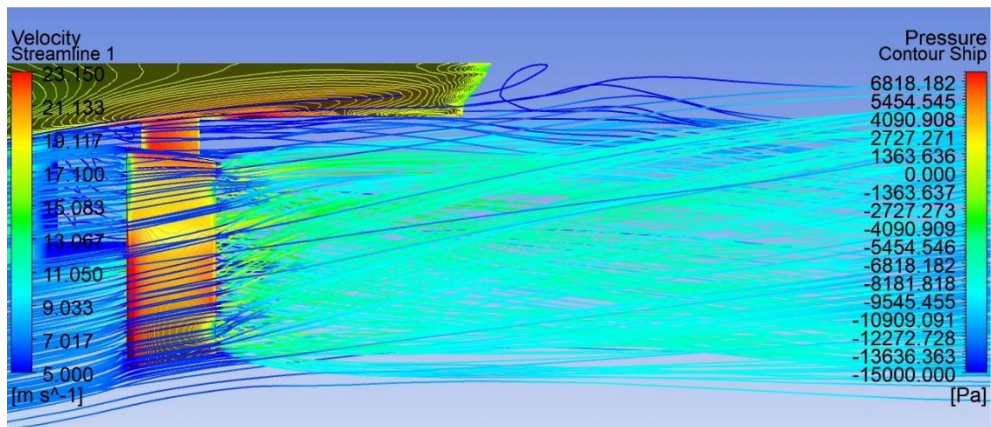
The simulation result stage allows users to view the visualization of the simulation results from any desired perspective. These visualizations can include representations of flow, pressure, temperature, or velocity on a model that has been altered with a variety of variables.



(a)



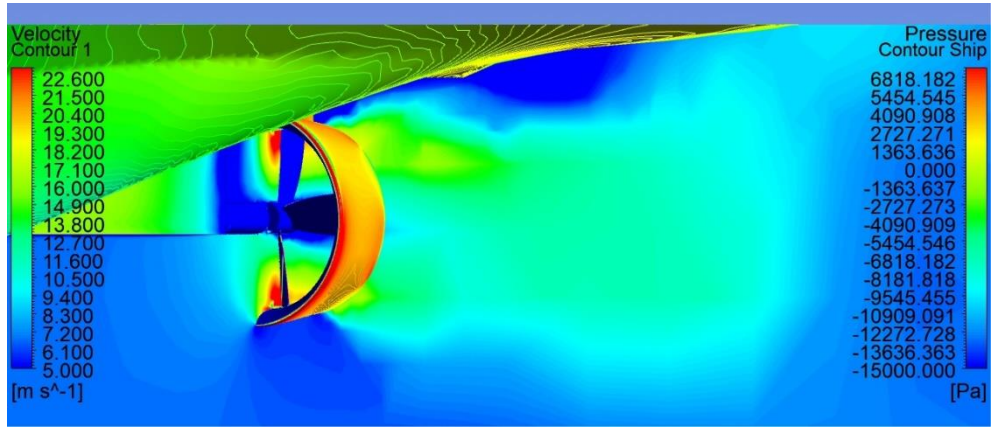
(b)



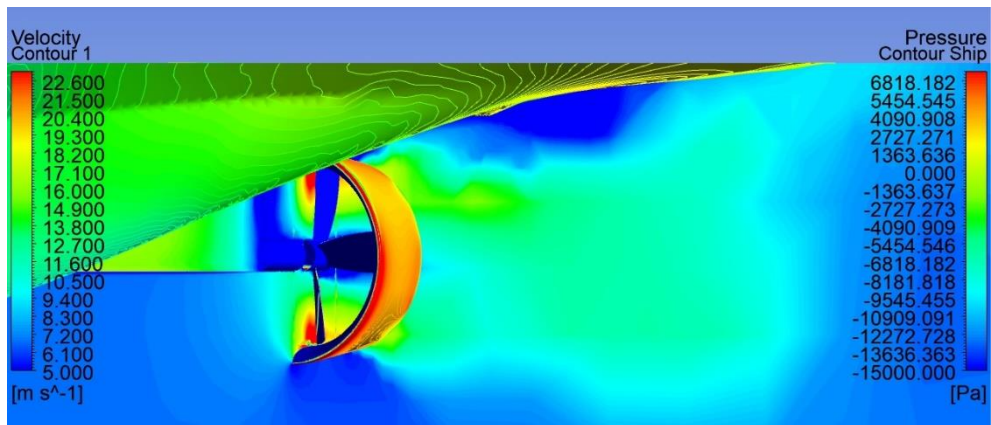
(c)

Figure 13. Velocity streamline (a) 10 mm (b) 20 mm (c) 30 mm

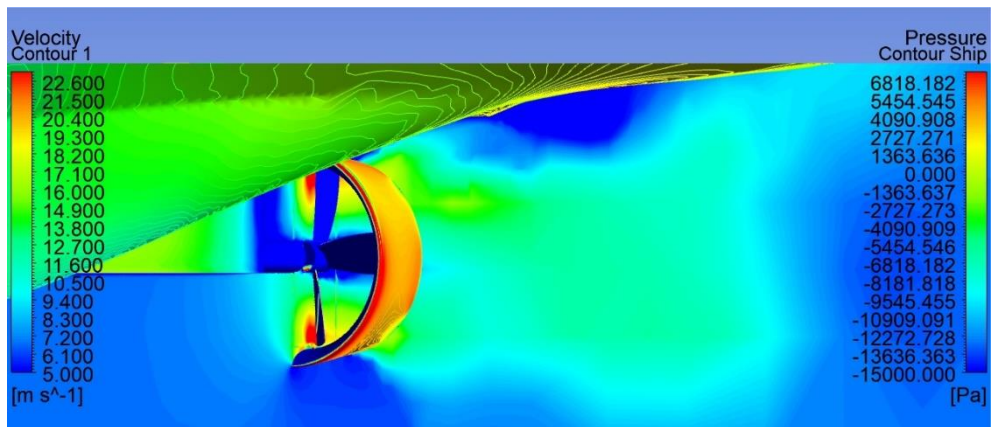
A streamline is a line that runs perpendicular to the direction of the instantaneous velocity. A streamline represents the path a zero-mass particle follows through the fluid domain. These streamlines start at each equally spaced node at a specific location. Another method for visualizing the airflow behavior needed for this investigation is using streamlines. Figure 13 shows the flow velocity distribution behind the ship. The highest velocity, reaching 19 m/s, is observed behind the propeller and is marked in yellow. As the flow moves away from the propeller, the velocity decreases to 9.033 m/s until it eventually reaches zero at a greater distance. This figure highlights that as the tip clearance distance gets smaller (e.g., at Figure 13 (a) 10 mm), the flow is more focused, and the velocity remains higher over longer distances, indicating an increase in propeller efficiency.



(a)



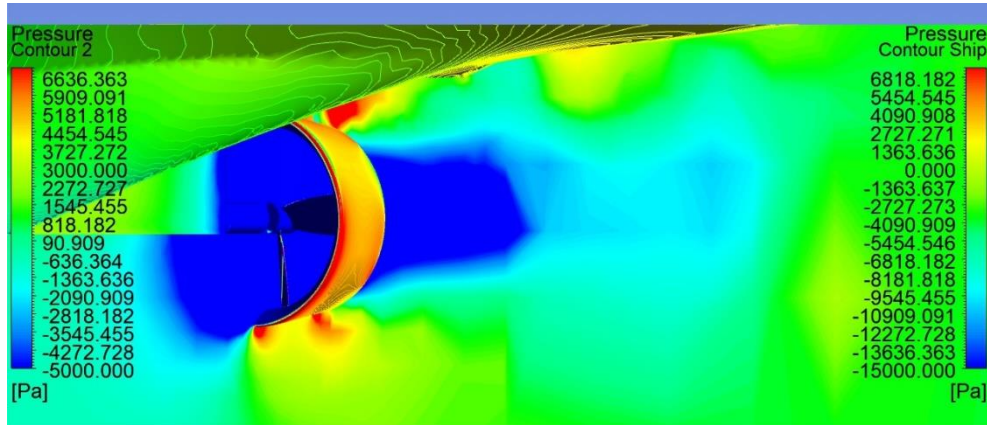
(b)



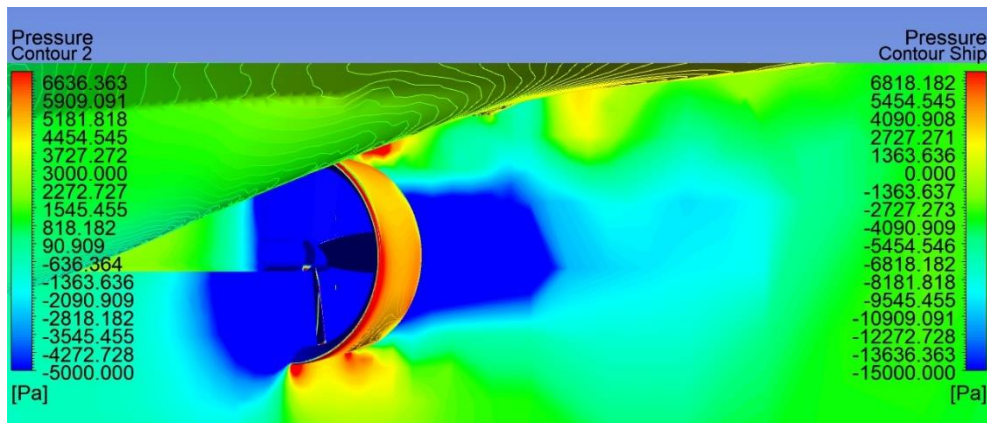
(c)

Figure 14. Velocity contour (a) 10 mm (b) 20 mm (c) 30 mm

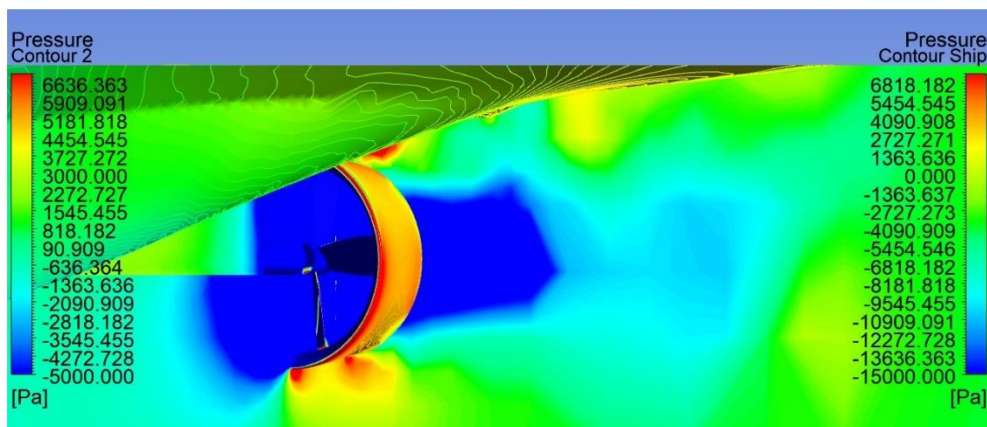
Figure 14 shows the flow velocity distribution around the propeller and Kort nozzle. The brighter color in the center indicates higher velocities, showing the effect of flow coalescence by the duct on the propeller. At a tip clearance of 10 mm, the flow is more focused and produces higher velocities in the center than with a larger clearance. This shows that a reduction in tip clearance can increase the efficiency of flow coalescence, providing greater thrust.



(a)



(b)



(c)

Figure 15. Pressure contour (a) 10 mm (b) 20 mm (c) 30 mm

Figure 15 shows the pressure distribution around the propeller and kort nozzle. The outside of the nozzle experiences higher pressure because the fluid flow outside is slower than the flow inside the nozzle. At smaller tip clearance (10 mm), the pressure difference is more significant, especially around the nozzle area. This means that the propeller works more efficiently, converting more fluid energy into thrust and torque. The higher the pressure values in the pressure contour and pressure contour ship indicators despite using the same indicator color (blue, which indicates negative or low pressure) can be explained by differences in the pressure scale. The blue color in the contour graph may represent a different range of pressure values in the pressure contour and pressure contour ship images. Although both images use blue to indicate low pressure, the absolute value range for pressure in the two images may be different. For example, blue on one image may represent a pressure of -1000 Pa, while on the other image, blue may represent a pressure of -500 Pa. This means that even though the indicator colors are the same, the pressure values are not identical. Overall, these figures show that the reduced tip clearance on the type 19A ducted propeller results in increased flow velocity and more effective pressure distribution around the propeller, which has a positive impact on increasing the thrust and torque of the vessel.

Following the study objectives, calculations were performed to evaluate the propeller's performance using simulated data. Thrust and torque calculations were conducted based on the propeller data. With a P/D value of 0.65, the pitch angle can be determined using eq. (9) [25].

$$\theta = \tan^{-1} \frac{P/D}{0,7\pi}$$

$$\theta = \tan^{-1} \frac{0,65}{0,7\pi}$$

$$\theta = 16,47^\circ$$

Lift and drag values were obtained from CFD post-simulation results. The thrust value is plotted on the graph by calculating lift and drag per eq. (6). Additionally, the pitch angle is determined. Torque, lift, and drag values are derived from simulation results. Torque is the force perpendicular to the propeller axis. To validate the simulation results, numerical calculations of thrust and torque are required. Table 3 compares thrust values from the Ansys simulation and numerical calculations. The thrust values from the Ansys simulation are generally lower than those from manual calculations, with a difference of less than 3% for each model variation.

Table 3. Comparison of Thrust Numerical Calculations and CFD Simulation

Model	Numerical Calculation (kN)	CFD Simulation (kN)	Difference (%)
10 mm	357,513	367,413	2,69
20 mm	355,952	365,459	2,60
30 mm	355,092	364,292	2,52
Without kort nozzle	340,339	337,921	0,71

This shows that the thrust results between the numerical calculation approach and the Computational Fluid Dynamics (CFD) simulation are not significantly different [26]. The 30 mm model has the lowest thrust force, while the 10 mm model has the highest thrust force. Table 3 shows the torque values between the numerical calculation and the Ansys simulation. The discrepancy between the torque values calculated manually and those obtained by the Ansys simulation is 1-2 percent for each model change.

Table 4. Comparison of Torque Numerical Calculations and CFD Simulation

Model	Numerical Calculation (kNm)	CFD Simulation (kNm)	Difference (%)
10 mm	308,691	315,338	2,10
20 mm	305,995	311,908	1,89
30 mm	304,124	311,023	2,21
Without kort nozzle	272,032	273,311	0,46

Table 4 presents the thrust and torque results from both simulations and numerical calculations, showing less than a 3% difference for each model variation. The 30 mm model has the lowest torque, while the 10 mm model has the highest. Graphs from Table 3 and Table 4 will be created to illustrate the calculation results for each model, providing a clearer understanding of the simulated models' characteristics. Figure 16 compares the thrust and torque of each model.

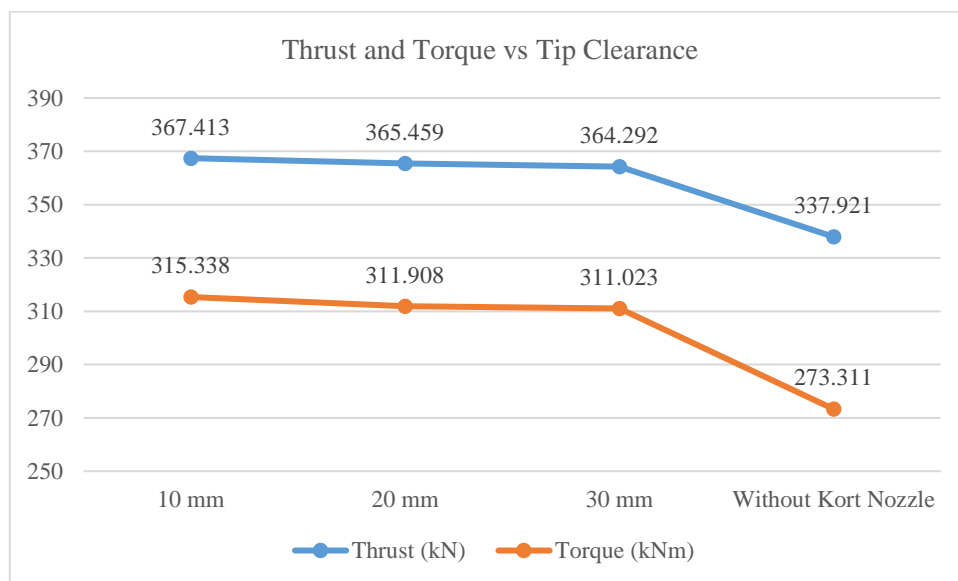


Figure 16. Thrust and Torque chart on 19A 10 mm, 20 mm, 30 mm, and without kort nozzle

The comparison graphs of thrust and torque on the 10 mm, 20 mm, 30 mm, and without kort nozzle models show that the thrust and torque values decrease the greater the value of the tip clearance of the kort nozzle. The 10 mm kort nozzle model can increase thrust by 8% and torque by 13,3%, then the 20 mm model can increase thrust by 7.5% and torque by 12.3%,

and the 30 mm model can increase thrust by 7.2% and torque by 12.1%. This shows that the installation of a MARIN foil 19A type Kort nozzle on an offshore supply vessel can cause a significant increase in thrust values, ranging from 7% to 8%, and can produce a considerable increase in torque values, ranging from 12% to 13%.

The findings show that the 10 mm model is the most effective among the three Kort nozzle models for increasing thrust and torque, achieving the highest results. Thus, it can be concluded that the Kort nozzle significantly impacts thrust and torque. The increase in thrust and torque is inversely proportional to the tip clearance value; smaller tip clearance results in higher thrust and torque due to the concentrated flow after passing through the rotating propeller.

4. Conclusion

All models used in this study yielded results; nozzle model 19A had the greatest thrust and torque, 367,413 kN and 315,338 kNm, while model 19A had the least thrust and torque, 364,292 kN and 311,023 kNm. There is an inverse correlation between tip clearance and thrust, which means that the greater the value of the tip clearance of the Kort nozzle used, the smaller the thrust generated. The correlation between tip clearance and torque also shows an inverse relationship, meaning that the greater the value of the tip clearance of the Kort nozzle used, the smaller the torque produced. For future research, angle of attack variations of the Kort nozzle can be investigated to understand the hydrodynamic characteristics of such differences. In addition, factors such as wind and current can also be incorporated into the study.

Acknowledgements

We would like to thank Hang Tuah University Surabaya for their assistance with this research. We also like to thank the fluid laboratory team for helping us with this research and providing the space and resources we needed.

References

- [1] Y. R. Andilolo, P. Manik, and M. Iqbal, "Studi Kasus Kinerja Propeller Kaplan Series Akibat Pengurangan Diameter dan Penambahan End Plate dengan Metode CFD," *Jurnal Teknik Perkapalan*, vol. 5, no. 1, pp. 205-213, 2017.
- [2] G. A. Putra and A. Winarno, "Studi Pengaruh Variasi Bentuk Wave-Piercing Terhadap Hambatan Pada Kapal Katamaran Untuk Meningkatkan Efisiensi Pemakaian Bahan Bakar," *Zona Laut: Jurnal Inovasi Sains dan Teknologi Kelautan*, vol. 3, no.1, pp. 24-31, 2022.
- [3] A. Winarno, G. Ciptadi, A. Iriany, and A. S. Widodo, "Experiment Study of the Resistance on Nusantara Ship Hull Modification with Fishing Boat in Pantura East Java," *International Journal on Engineering Applications*, vol. 11, no. 2, pp. 111-120, 2023.
- [4] A. Winarno, G. Ciptadi, A. Iriany, and A. S. Widodo, "Experimental and Numerical Study of Ship Resistance on the Combination of Traditional Nusantara Fishing Vessel Hull Forms," *International Review of Mechanical Engineering*, vol. 17, no.4, pp. 190-196, 2023.
- [5] W. Rakhmadi, A. Trimulyono, and M. Iqbal, "Analisa Perbandingan Tipe Kort Nozzle Terhadap Gaya Dorong Propeller Dengan Metode CFD," *Jurnal Teknik Perkapalan*, vol. 4, no. 1, pp. 199-208, 2016.
- [6] D. N. Yunita and A. Winarno, "Analisa Teknis Pengaruh Jumlah Sudu Propeller Bebas Putar Terhadap Gaya Dorong Kapal Tunda DPS IX," Seminar Nasional Kelautan XIV: Implementasi Hasil Riset Sumber Daya Laut dan Pesisir Dalam Peningkatan Daya Saing Indonesia, 2019.
- [7] M. F. Rozi, A. Winarno, and M. Riyadi, "Pengaruh Variasi Jarak Poros Propeller Yang Berbeda Pada Kapal Ikan Tradisional KM. Sri Mulyo di Brondong Lamongan," Seminar Nasional Kelautan XIV: Implementasi Hasil Riset Sumber Daya Laut dan Pesisir Dalam Peningkatan Daya Saing Indonesia, 2019.
- [8] A. F. Rachmat, A. Trimulyono, and P. Manik, "Analisa Pengaruh Pemasangan Energy Saving Device (ESD) Jenis Mewis Duct Terhadap Thrust Propeller INSEAN E779A Dengan Menggunakan Pendekatan CFD," *Jurnal Teknik Perkapalan*, vol. 9, no. 3, pp. 294-302, 2021.
- [9] M. Oosterveld, "Wake adapted ducted propellers," Netherlands Ship Model Basin, 1970.
- [10] C. Negrato, "Prediction of The Performance of Ducted Propellers With BEM and Hybrid RANS-BEM Methods," Delft University of Technology, 2015.
- [11] R. M. Khozin, "Pengaruh Variasi Pitch Terhadap Kinerja Ducted Contra Rotating Propeller Dengan Pendekatan CFD," Institut Teknologi Sepuluh November, 2016.
- [12] H. Schneekluth and V. Betram, "Ship Design for Efficiency and Economy," Oxford: Butter Worth Heinmann, 1998.
- [13] M. D. Maulana, A. F. Zakki, and P. Manik, "Analisa Performance Propeller Tipe KA4-70 dengan Variasi Flap Angle End Plate dan Sudut Rake," *Jurnal Teknik Perkapalan*, vol. 8, no. 1, pp. 11-20, 2020.
- [14] D. Yongle, S. Baowei, and W. Peng, "Numerical Investigation of Tip Clearance Effects on The Performance of Ducted Propeller," *International Journal of Naval Architecture and Ocean Engineering*, vol. 7, pp. 795-804, 2015.
- [15] M. A. R. Hermawan and A. Winarno, "Kajian Teknis Propeller Tipe B - Series Dan Kaplan Dengan Variasi Sudut Rake Pada Kapal Offshore Supply Vessel 80 (OSV 80)," *Zona Laut: Jurnal Inovasi Sains dan Teknologi Kelautan*, vol. 4, no. 3, pp. 309-318, 2023.

- [16] W. N. R. Ahmidilla, "Analisa Penerapan Kort Nozzle Untuk Propeller B4-40 Kapal Offshore Supply Vessel (OSV)," Univeristas Hang Tuah, 2024.
- [17] P. I. Adyanata and A. Winarno, "Kajian Teknis Penggunaan Hub dan Hubless Rim Driven Propeller (Rdp) Sebagai Propeller Kapal Di Perairan Dangkal," *Jurnal Inovtek Polbeng*, vol. 12, no. 1, 2022.
- [18] J. Carlton, "Marine Propellers and Propulsion," Oxford: Elsevier Ltd. All right reserved, 2007.
- [19] E. P. Popov, "Mechanic of Materials." San Francisco. Berkeley, 1984.
- [20] A. R. Nuranto, A. J. Fitroh, and H. Syamsudin, "Analysis of Aerodynamic Load of LSU-03 (LAPAN Surveillance UAV-03) Propeller," 5th International Seminar of Aerospace Science and Technology, *IOP Conf. Series: Journal of Physics: Conf. Series*, 2018.
- [21] M. H. Firmansyah, "Studi Perbandingan Penerapan Haluan Axe Bow Dengan Ulstein X-Bow Pada Kapal Offshore Supply Vessel (OSV) 80 Terhadap Hambatan Total," Universitas Hang Tuah, 2023.
- [22] X. Zhang, Z. Liu, L. Cao, and D. Wan, "Tip Clearance Effect on The Tip Leakage Vortex Evolution and Wake Instability of a Ducted Propeller," *Journal of Marine Science and Engineering*, vol. 8, no. 8, 2022.
- [23] Ansys, "ANSYS Fluent Mosaic Technology Automatically Combines Disparate Meshes with Polyhedral Elements for Fast, Accurate Flow Resolution," Ansys, Inc. All Rights Reserved, 2020.
- [24] F. R. Menter, R. Lechner, and A. Matyushenko, "Best Practice: RANS Turbulence Modeling in Ansys CFD," Ansys, Inc. All Rights Reserved, 2021.
- [25] I. S. Arief, T. B. Musriyadi, and A. D. A. J. Mafera, "Analysis Effect of Duct Length- Nozzle Diameter Ratio and Tip Clearance Variation on the Performance of K-Series Propeller," *International Journal of Marine Engineering Innovation and Research*, vol. 2, no. 1, pp. 77-85, 2017.
- [26] A. Winarno, A. S. Widodo, G. Ciptadi, and A. Iriany, "The Effect of Sail Layout on Fishing Vessels Hydrodynamics in the North Coast of Java using Computational Fluids Dynamic," *CFD Letter*, vol. 16, issue. 1, pp. 107-120, 2024.
- [27] M. H. Firmansyah, "Studi Perbandingan Penerapan Haluan Axe Bow Dengan Ulstein X-Bow Pada Kapal Offshore Supply Vessel (OSV) 80 Terhadap Hambatan Total," Universitas Hang Tuah, 2023.